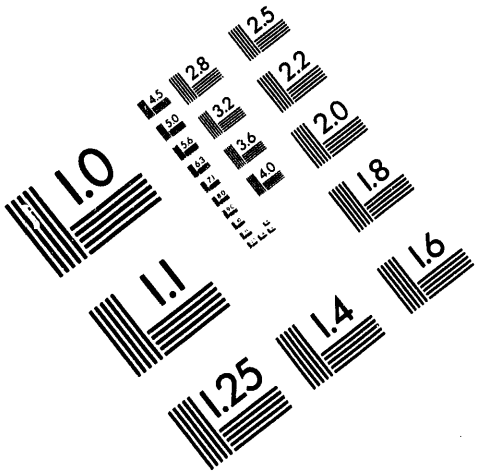

Association for Information and Image Management

1100 Wayne Avenue, Suite 1100
Silver Spring, Maryland 20910

301/587-8202

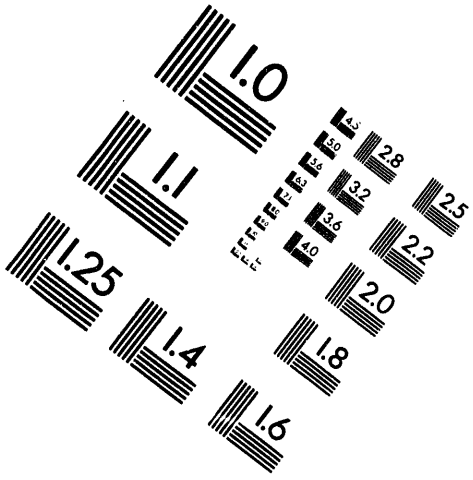

Centimeter

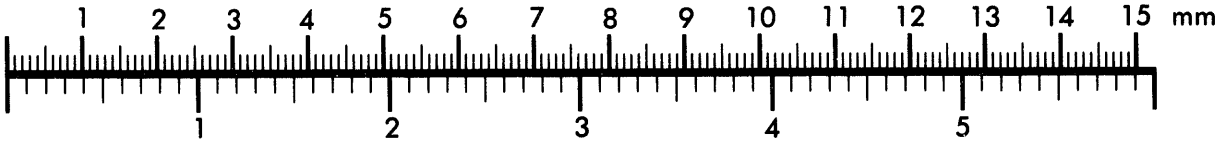

Inches

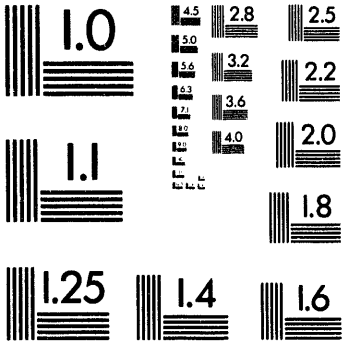

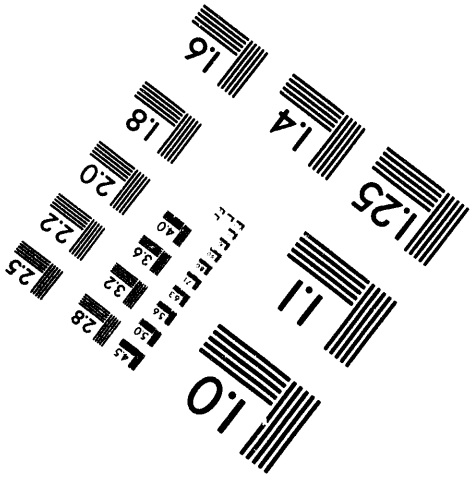

MANUFACTURED TO AIIM STANDARDS
BY APPLIED IMAGE, INC.

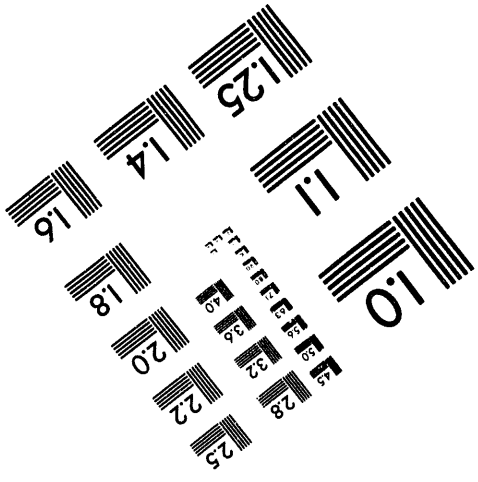

1 of 1

2

SAND--94-8704C
Conf-941142--16

THE MODIFIED EMBEDDED ATOM METHOD

M. I. Baskes
Sandia National Laboratories
Livermore, CA 94550

DISCLAIMER

This report was prepared as an account of work sponsored by an agency of the United States Government. Neither the United States Government nor any agency thereof, nor any of their employees, makes any warranty, express or implied, or assumes any legal liability or responsibility for the accuracy, completeness, or usefulness of any information, apparatus, product, or process disclosed, or represents that its use would not infringe privately owned rights. Reference herein to any specific commercial product, process, or service by trade name, trademark, manufacturer, or otherwise does not necessarily constitute or imply its endorsement, recommendation, or favoring by the United States Government or any agency thereof. The views and opinions of authors expressed herein do not necessarily state or reflect those of the United States Government or any agency thereof.

ABSTRACT

Recent modifications have been made to generalize the Embedded Atom Method (EAM) to describe bonding in diverse materials. By including angular dependence of the electron density in an empirical way, the Modified Embedded Atom Method (MEAM) has been able to reproduce the basic energetic and structural properties of 45 elements. This method is ideally suited for examining the interfacial behavior of dissimilar materials.

This paper will explain in detail the derivation of the method, show how the parameters of the MEAM are determined directly from experiment or first principles calculations, and examine the quality of the reproduction of the database.

Materials with fcc, bcc, hcp, and diamond cubic crystal structure will be discussed. A few simple examples of the application of the MEAM to surfaces and interfaces will be presented. Calculations of pullout of a SiC fiber in a diamond matrix as a function of applied stress show non-uniform deformation of the fiber.

INTRODUCTION

Empirical and semi-empirical computational methods for metals and covalent materials have evolved rapidly in the past few years. These methods have recently been reviewed by Carlsson (Ref. 13), in an MRS Symposium (Ref. 35), and at a special symposium of the World Materials Congress (Ref. 37). The Embedded Atom Method (EAM) has been the mainstay of the new methods used for metallic systems. Daw and Baskes (Refs. 13, 14) introduced this method over a decade ago. The EAM, which is based on density functional theory, has successfully been applied to the fcc or nearly-filled d-band transition metals and also to bcc metals (Refs. 1, 28). A number of recent papers summarize the technique and its many applications (Refs. 5, 6, 14, 15, 17, 18, 21, 22, 23). Finnis and Sinclair (Ref. 20) derived a similar method based on a second moment approximation to tight binding and originally applied it to the bcc or half-filled d-band transition metals.

A basic limitation of the EAM is that it spherically averages the electron density which precludes directional bonding. Baskes (Ref. 2) modified the EAM to include directional

MASTER

DISTRIBUTION OF THIS DOCUMENT IS UNLIMITED

bonding and applied it to silicon. The silicon EAM model was extended by Baskes, et al. (Ref. 8) to the silicon/germanium system where the Modified Embedded Atom Method (MEAM) was developed. Most recently the MEAM has been extended to fcc, bcc (Ref. 3) and hcp (Ref. 7) metals. Savino et al. (Ref. 34) developed a related method based on second order invariants.

All of these methods are mathematically similar and have in common the attribute that the interaction between two atoms depends upon their local environment. It is mainly this fact that accounts for the success that these methods have had in predicting effects at metallic surfaces where the atomic environment is significantly different from the bulk.

This paper will review the derivation of the MEAM and its application to a large number of elements showing its wide range of applicability. An underlying theme in the development of the method is computational simplicity so that the interactions may be readily used for large molecular dynamics or Monte Carlo simulations. MEAM functions for the Si/C system will be developed and applied to the deformation of a SiC fiber in a diamond matrix.

THEORY

The total energy E of a system of atoms in the Embedded Atom Method (EAM) has been shown (Ref. 16) to be given by an approximation of the form:

$$E = \sum_i \left(F_i(\bar{\rho}_i) + \tfrac{1}{2} \sum_{j \neq i} \phi_{ij}(R_{ij}) \right) \tag{1}$$

where the sums are over the atoms i and j.* In this approximation, the embedding function F_i is the energy to embed an atom of type i into the background electron density at site i, $\bar{\rho}_i$; and ϕ_{ij} is a pair interaction between atoms i and j whose separation is given by R_{ij}. In the EAM, $\bar{\rho}_i$ is given by a linear supposition of spherically averaged atomic electron densities, while in the Modified Embedded Atom Method (MEAM), $\bar{\rho}_i$ is augmented by angularly dependent terms (Refs. 2, 3, 7, 8). Let us denote the term in brackets in Eq. 1, i.e., the direct contribution to the energy from the ith atom, as E_i. Of course, atom i also indirectly contributes to the energy through its interactions with its neighbors. Then E_i may be written as follows:

$$E_i = F_i(\bar{\rho}_i) + \tfrac{1}{2} \sum_{j \neq i} \phi_{ij}(R_{ij}). \tag{2}$$

As in Baskes et al. (Refs. 3, 8) consider the case of a homogeneous monatomic solid with interactions limited to first neighbors only. In a specific reference structure (usually the equilibrium structure) for an atom of type i we have:

$$E_i^u(R) = F_i(\bar{\rho}_i^0(R)) + \tfrac{1}{2} Z_i \phi_{ii}(R) \tag{3}$$

where $\bar{\rho}_i^0(R)$ is the background electron density for the reference structure of atom i, Z_i is the coordination, and R is the nearest neighbor distance. Here $E_i^u(R)$ is the energy per atom of the reference structure as a function of nearest neighbor distance, obtained, e.g., from first principles calculations or the universal equation of state of Rose et al. (Ref. 32). Here we choose the latter:

*Throughout the paper the subscripts (i,j,k) denote either an atom at a particular site or the type of that atom.

$$E_i^u(R) = -E_c\left(1+\alpha\left(\frac{R}{r_e}-1\right)\right)e^{-\alpha(R/r_e-1)} \tag{4}$$

with

$$\alpha^2 = \frac{9\Omega B}{E_c} \tag{5}$$

where E_c, r_e, Ω, and B are the cohesive energy, nearest-neighbor distance, atomic volume, and bulk modulus, respectively, all evaluated at equilibrium in the reference state. The pair potential for like atoms is then given by:

$$\phi_{ii}(R) = \frac{2}{Z_i}\left\{E_i^u(R) - F_i(\bar{\rho}_i^0(R))\right\}. \tag{6}$$

At equilibrium (denoted by $|_{r_e}$), with the use of this form, $E|_{r_e} = -E_c$, $dE/dr|_{r_e} = 0$, and $d^2E/dr^2|_{r_e} = 9\Omega B/r_e^2$ so that agreement is assured between the model and the input cohesive energy, atomic volume, and bulk modulus. The pair potential for unlike atom pairs will be discussed below.

In the MEAM the embedding function F (ρ) is taken as

$$F(\rho) = AE_c\frac{\rho}{\rho_0}\ln\frac{\rho}{\rho_0} \tag{7}$$

where A is an adjustable parameter and ρ_0 is a density scaling parameter. See Baskes et al. (Refs. 2, 8) for a justification of this functional form. The density scaling parameter was initially (Ref. 3) taken to be the coordination times the atomic density scaling factor (see Eq. 11 below) and more recently (Ref. 7) as the density in the equilibrium reference structure. The SiC calculations presented below use the latter definition. For fcc and bcc reference lattices the definitions are identical. For hcp and diamond cubic there is a small difference.

The background electron density, $\bar{\rho}_i$, is assumed to be a function of what we call partial electron densities. These partial electron densities contain the angular information in the model. The reader should be cautioned that even though the electron density may be thought of as qualitatively similar to a real electron density, there is no expectation that the electron densities calculated here would be in agreement with those obtained from first principles calculations. A number of functional forms have been used previously (Refs. 2, 3, 4, 7, 8).

For example, the square of the electron density at a given site has previously (Ref. 3) been defined as the sum of terms with s, p, d, and f symmetry from the neighboring atoms. By including these angular terms in the background electron density, we introduce angular forces into the model. Thus at a particular atom:

$$\bar{\rho}^2 = \sum_{h=0}^{3} t^{(h)}\rho^{(h)2} \tag{8}$$

with h=0 to 3 corresponding to s, p, d, and f symmetry, respectively, and for convenience we take $t^{(0)} = 1$. We note that in a crystal the s, p, d, and f terms may be considered as measures of volume, polarization, shear, and lack of inversion symmetry, respectively. For example, as we vary the volume of a perfect fcc lattice, only $\rho^{(0)}$ is not equal to zero and, thus, it can simply be related to the volume. Similarly as we shear the fcc lattice, contributions from $\rho^{(2)}$ arise. An

alternative exponential form with the same asymptotic behavior near the perfect lattice has also been used (Ref. 7):

$$\bar{\rho} = \rho^{(0)} e^{\left[\frac{1}{2}\sum_{h=1}^{3} t^{(h)} (\rho^{(h)}/\rho^{(0)})^2\right]}. \tag{9}$$

The contributions to the density are given by:

$$\rho^{(0)} = \sum_i \rho^{a(0)}(r^i) \tag{10a}$$

$$(\rho^{(1)})^2 = \sum_\alpha \left[\sum_i \rho^{a(1)}(r^i)\frac{r_\alpha^i}{r^i}\right]^2 \tag{10b}$$

$$(\rho^{(2)})^2 = \sum_{\alpha,\beta}\left[\sum_i \rho^{a(2)}(r^i)\frac{r_\alpha^i r_\beta^i}{r^{i\,2}}\right]^2 - \tfrac{1}{3}\left[\sum_i \rho^{a(2)}(r^i)\right]^2 \tag{10c}$$

$$(\rho^{(3)})^2 = \sum_{\alpha,\beta,\gamma}\left[\sum_i \rho^{a(3)}(r^i)\frac{r_\alpha^i r_\beta^i r_\gamma^i}{r^{i\,3}}\right]^2. \tag{10d}$$

Here, the $\rho^{a(h)}$ are radial functions which represent the decrease in the contribution with distance r^i from the site in question, the superscript i indicates neighboring atoms to the site in question, and the α, β, and γ summations are each over the three coordinate directions with r_α^i being the distance from the site in question in that direction. The functional forms for the partial electron densities (h=1,3) were chosen to be translationally and rotationally invariant and equal to zero for crystals with cubic symmetry. Finally, the individual contributions are assumed to decrease exponentially, i.e.,

$$\rho^{a(h)}(R) = \rho_0^a e^{-\beta^{(h)}(R/r_e - 1)} \tag{11}$$

where ρ_0^a and $\beta^{(h)}$ are constants. For alloys the coefficients $t^{(h)}$ were initially assumed to depend on the properties of the atom at which the average electron density was calculated (Ref. 3). More recently (Ref. 26) it has been found that better agreement with defect properties in SiC could be obtained if the properties of the atoms surrounding this atom were included. The latter averaging procedure is used below for the SiC calculations:

$$t^{(h)} = \sum_i t_i^{(h)} \rho_0^{a(0)} / \rho^{(0)}. \tag{12}$$

The determination of the parameters has been discussed previously (Refs. 3, 7) in great detail. Basically, analytic expressions are obtained for the elastic constants, vacancy formation energy, and structural energy differences. Using these expressions and experimental data each parameter (or sets of parameters) is uniquely defined. The relationship between the parameters and the experimental input is summarized in Table 1. A number of the β parameters are not well determined for the fcc and bcc elements and nominal values are chosen for convenience.

Table 1 - Parameters and their correspondence with experimental data.

Parameter	Experimental Input
E_c	sublimation energy
r_e	atomic volume
α	bulk modulus
A	structural energy difference
$\beta^{(0)}$, $t^{(2)}$	shear moduli
$\beta^{(1)}$	internal relaxation for hcp
$\beta^{(2)}$, $\beta^{(3)}$	shear moduli for hcp
$t^{(1)}$	vacancy formation energy
$t^{(3)}$	stacking fault energy or c/a for hcp

RESULTS AND DISCUSSION

We begin this section with a diagram of the periodic table that shows the elements for which MEAM functions have been developed. These functions are now available for the 45 elements denoted by shaded squares. As you can see in Fig. 1, MEAM functions exist for most of the

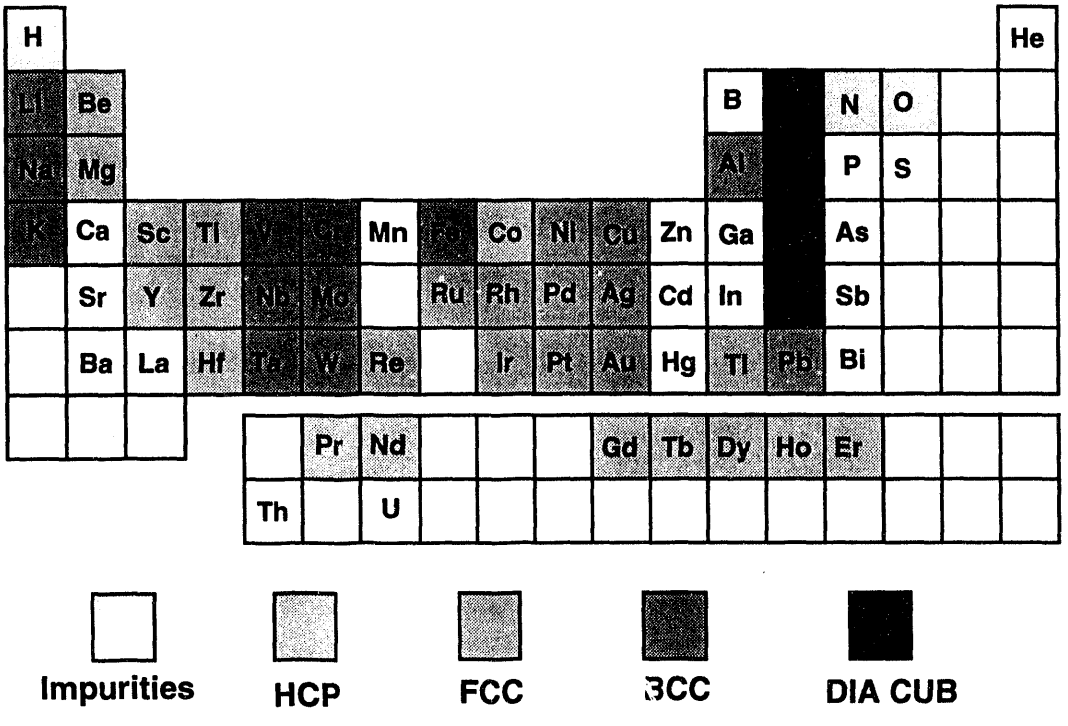

Figure 1 - Periodic table of the elements showing the current status of MEAM function development. The shaded squares denote those elements for which MEAM functions currently exist.

technologically interesting elements. We are currently in the process of developing MEAM functions for the additional elements whose names are present in unshaded squares. It should be

noted that once functions are available for a pair of elements it is relatively simple to produce the pair interactions so that alloy or compound calculations may be performed. We have no current interest in the other elements in the table.

To examine the ability of the MEAM to represent the properties of "real materials" a number of examples are presented. The MEAM parameters used here are those previously presented (Refs. 3, 7). As a first example the surface energy of a number of materials is shown in Fig. 2. Here we plot the calculated surface energy of a (100) face using MEAM vs. the experimental value of an "average" surface extrapolated to 0 K. Also included in the "experimental" data set are calculated estimates from de Boer, et al. (Ref. 19). As the figure shows the agreement with experiment is quite good for most of the elements. In contrast, EAM calculations of surface energy (Ref. 24) are frequently in disagreement with experiment by up to 40%.

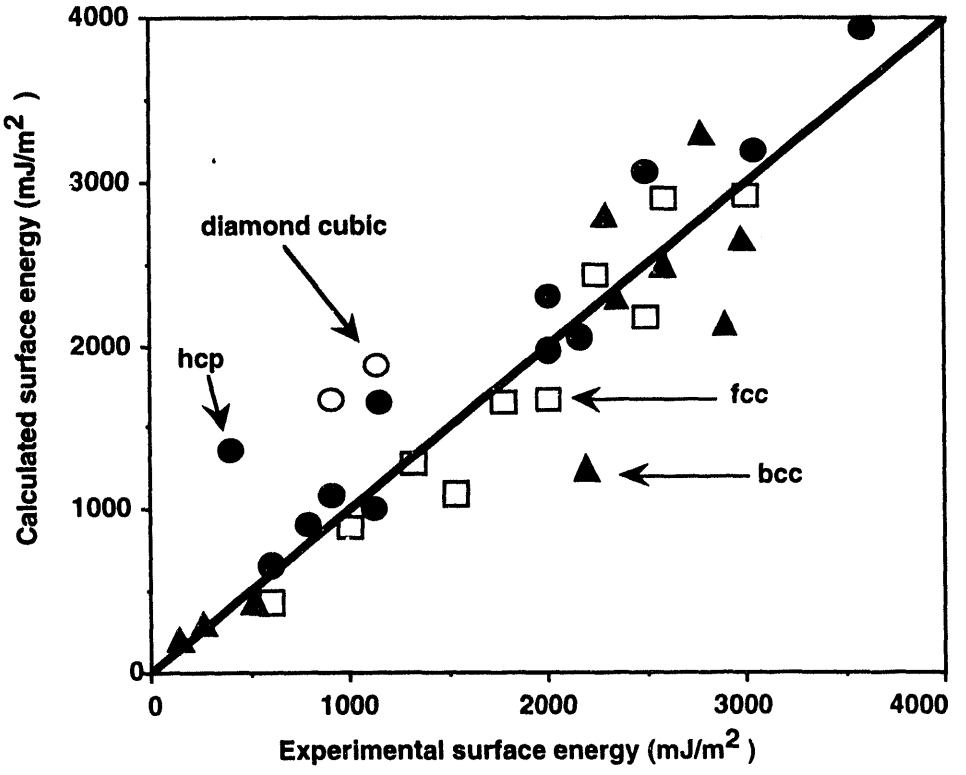

Figure 2 - Comparison of experimental (Refs. 19, 27, 36) and calculated surface energies for various elements. The elements shown are those denoted in Fig. 1.

As a second example calculated structural energies are shown in Fig. 3. The energies shown in the figure are those obtained after minimization with respect to lattice constant. The calculations are compared to an estimate of structural energy differences derived from analyses of experimental phase diagrams (Ref. 33), stacking fault energies (Refs. 25, 29, 31) and first principles calculations (Ref. 30).

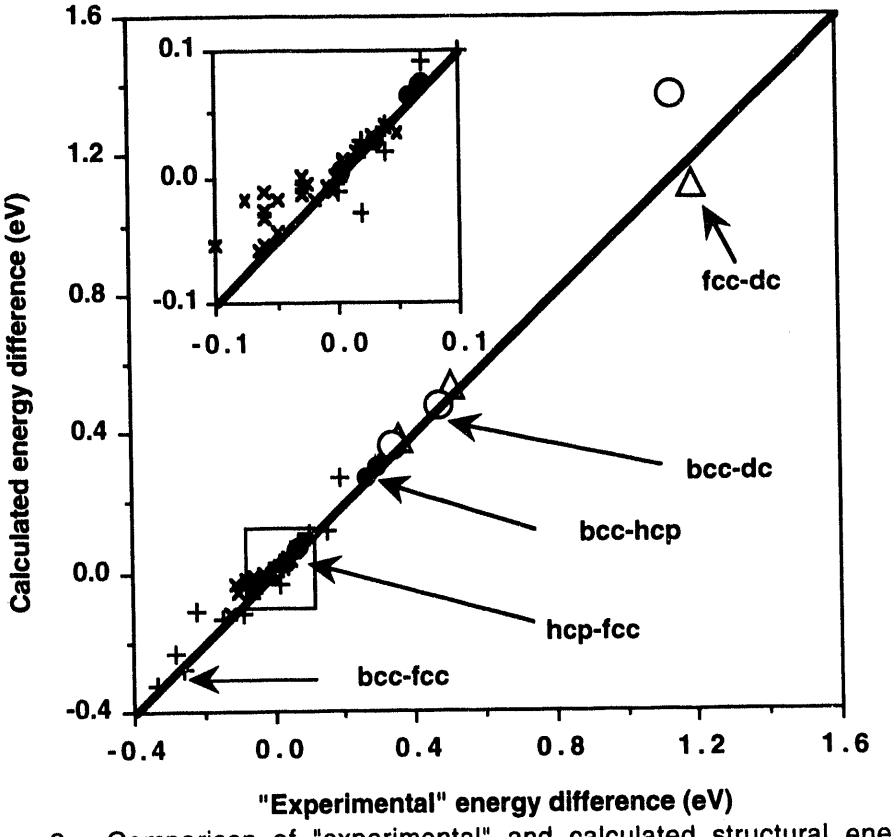

Figure 3 - Comparison of "experimental" and calculated structural energy differences for various elements. The elements shown are those denoted in Fig. 1. See text for how the "experimental" values are determined. The inset shows the detail for very small energy differences.

The final example is that of a small SiC fiber embedded in a matrix of diamond. The MEAM potentials for silicon and carbon have been modified slightly from those previously developed (Ref. 3) to include use of the exponential form for the average electron density and more recent elastic constants of carbon (Ref. 38). The parameters for the new potentials are given in Table 2.

Table 2 - Parameters for the MEAM

Values listed are the cohesive energy E_c (eV), the equilibrium nearest neighbor distance r_e (Å), the exponential decay factor for the universal energy function α, the scaling factor for the embedding energy A, the exponential decay factors for the atomic densities $\beta^{(i)}$, the weighting factors for the atomic densities $t^{(i)}$, and the density scaling factor ρ_0^a.

	E_c	r_e	α	A	$\beta^{(0)}$	$\beta^{(1)}$	$\beta^{(2)}$	$\beta^{(3)}$	$t^{(1)}$	$t^{(2)}$	$t^{(3)}$	ρ_0^a
C	7.37	1.54	4.38	1.0	4.1	4.2	5.0	3.0	5.0	9.34	-1.0	2.5
Si	4.63	2.35	4.87	1.0	4.8	4.8	4.8	4.8	3.3	5.11	-0.8	1.0
SiC	6.43	1.89	4.37	-	-	-	-	-	-	-	-	-

In Table 3 the elastic constants and vacancy formation energy calculated from these functions are compared to experiment. Agreement is excellent.

Table 3 - Elastic constants and vacancy formation energies for C and Si.

The experimental elastic constants are from Refs. 10 and 38 and the first principles calculations of vacancy formation energies are from Refs. 9, 11, and 12.

	c_{11} (eV/Å^3)		c_{12} (eV/Å^3)		c_{44} (eV/Å^3)		E^f_{1v} (eV)	
	Calc.	Expt.	Calc.	Expt.	Calc.	Expt.	Calc.	Theory
C	6.77	6.74	0.77	0.78	3.66	3.61	6.5	7.2
Si	1.01	1.03	0.41	0.40	0.46	0.48	3.0	5 - 6

The reference state for the alloy system is taken to be the diamond cubic structure (β) of SiC. The parameters for the equation of state are given in Table 2. Using a method similar to that described in Baskes (Ref. 3), the following expression is obtained for the Si-C pair potential:

$$\phi_{\mathrm{SiC}} = \frac{1}{4}\left\{2E^{u}_{\mathrm{SiC}} - F_{\mathrm{C}}(\bar{\rho}^{0}_{\mathrm{C}}) - F_{\mathrm{Si}}(\bar{\rho}^{0}_{\mathrm{Si}})\right\}, \tag{13}$$

where

$$\bar{\rho}^{0}_{\mathrm{C}} = 4\rho^{a(0)}_{\mathrm{Si}} e^{\frac{1}{9}t^{a(3)}_{\mathrm{Si}}(\rho^{a(3)}_{\mathrm{Si}}/\rho^{a(0)}_{\mathrm{Si}})^2} \tag{14}$$

and

$$\bar{\rho}^{0}_{\mathrm{Si}} = 4\rho^{a(0)}_{\mathrm{C}} e^{\frac{1}{9}t^{a(3)}_{\mathrm{C}}(\rho^{a(3)}_{\mathrm{C}}/\rho^{a(0)}_{\mathrm{C}})^2} \tag{15}$$

The elastic constants of SiC using the above potentials are calculated to be: bulk modulus 1.32 eV/Å^3; shear modulus (c_{44}) 1..28 eV/Å^3; and second shear modulus 0.89 eV/Å^3. By construction the cohesive energy, lattice constant, and bulk modulus agree exactly with experiment.

Calculations were performed to simulate the deformation of a SiC fiber in a diamond carbon (C) matrix. The geometry is shown in Fig. 4. Both the SiC and C are single crystals with a (100) orientation. The computational cell is about 40 Å long in the axial direction which is 11 unit cells of C and 9 unit cells of SiC. Choosing this ratio of cells allows almost perfect matching of the periodicity of the C and SiC. The SiC fiber is 10 Å in diameter. The surrounding C matrix is effectively infinite in radial extent with C atoms outside of a 20 Å diameter cylinder held fixed in space. The fiber/matrix cell is allowed to relax to its minimum energy configuration. To restrict interactions to first neighbors, screening is included as in Ref. 7. Axial forces are then applied to each atom of the SiC fiber and the atoms are allowed to relax to their minimum energy configuration.

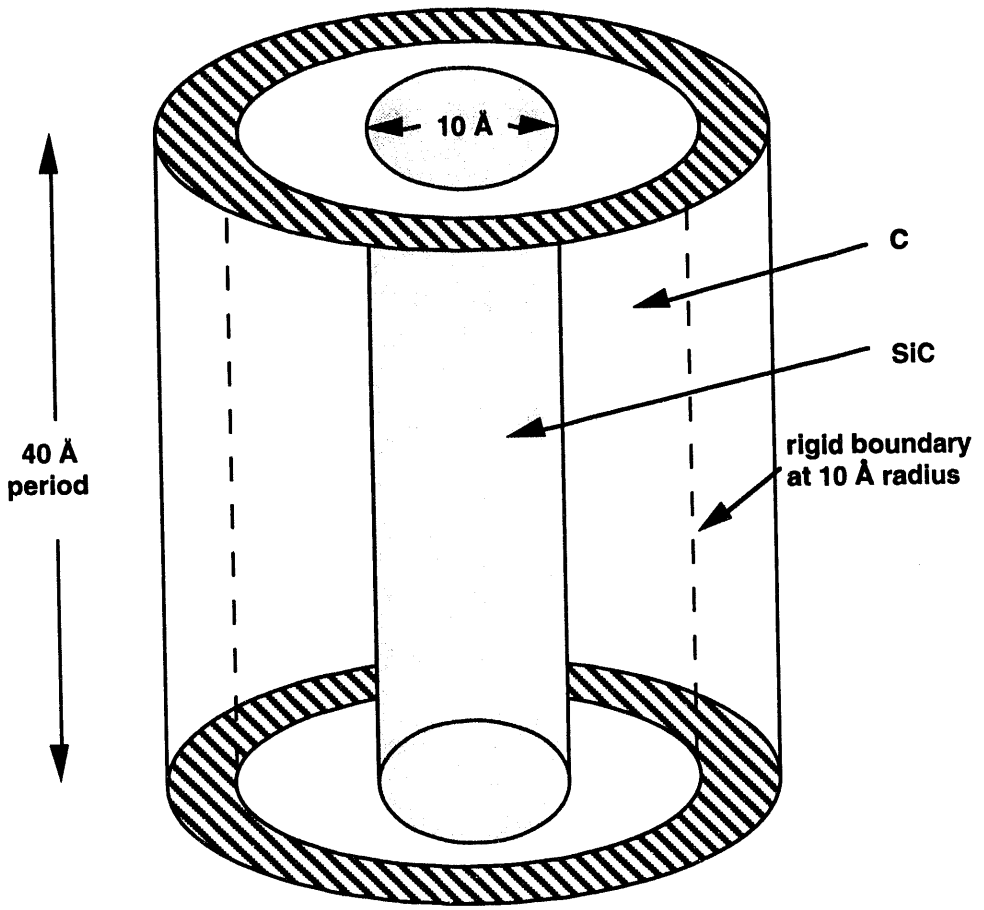

Figure 4 - Geometry of the SiC fiber in a C matrix.

In Fig. 5 we see the resulting displacement of the fiber and matrix atoms. The displacement is relatively constant across the fiber and decreases rapidly in the matrix. A significant amount of shear occurs in the fiber near the fiber/matrix interface. If we assume that the applied force, f, acts directly on the matrix, in a continuum model the predicted displacement in the matrix, d, at a radial position, r, is given by:

$$d = \frac{f(R-r)}{A_0 C_{44}} \tag{16}$$

where R is the position of the fixed boundary (10Å) and A_0 is the area (6.32Å^2/atom) that the force acts on. The predicted displacement, as shown in Fig. 5, is in excellent agreement with the atomistic calculation. At the higher forces the displacement near the interface is somewhat under predicted by the continuum calculation.

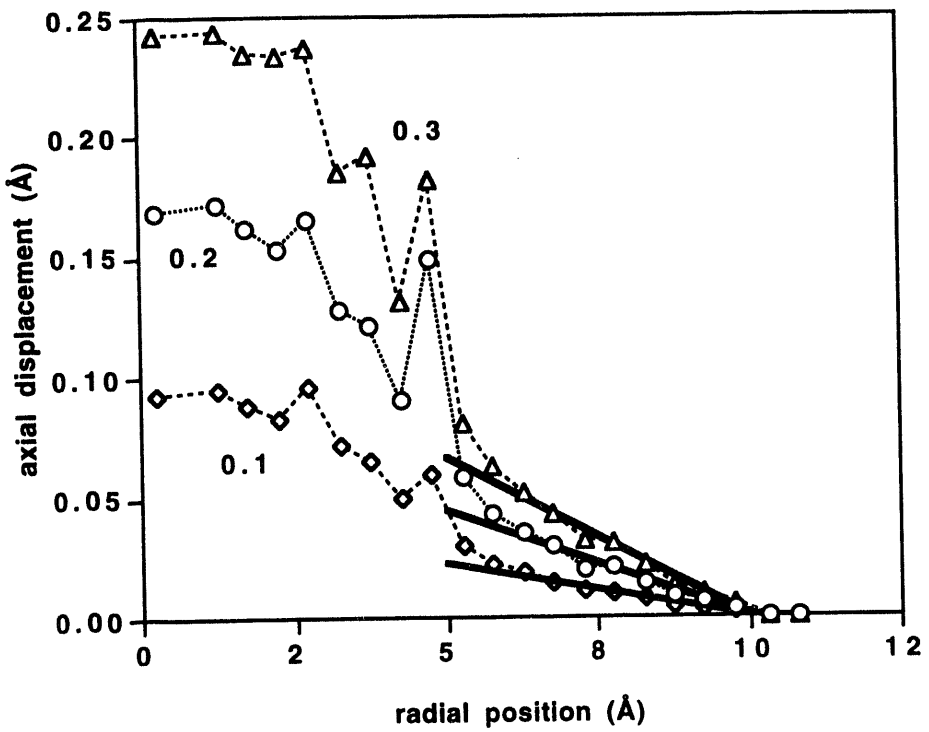

Figure 5 - Axial displacement as a function of radial position. The fiber boundary is at 5 Å. Curves are labeled by the applied axial force (eV/Å/atom). The solid lines represent the displacements predicted by a rigid continuum model (Eq. 16).

We have investigated the uniformity of displacement in the fiber and matrix. In a continuum model one would expect a uniform displacement field throughout the length of the computational cell. In the atomistic calculation, however, the SiC/C boundary structure varies as we move along the axial direction potentially leading to regions of different adhesion. In essence we have introduced dislocations into the interface to account for the mismatch in the SiC and diamond lattice constants. We clearly see this effect in Fig. 6 *(a)*. Here we show the axial displacement as a function of axial position for the case of the applied axial force of 0.3 eV/Å/atom. Away from the interface the displacements are relatively uniform as expected from continuum theory. However, the displacements in the SiC fiber near the interface (r=2.75 and 4.25 Å) vary by almost a factor of two. A region of large displacements occur near the center of the periodic fiber. The fact that the displacements show a minimum at the boundary of the periodic cell is related to the specific boundary structure. At this axial position the C and SiC share a common plane most likely leading to higher adhesion and hence smaller displacements.

Similarly the SiC/C boundary structure varies circumferentially. In Fig. 6 *(b)* we see that the axial displacements do not vary much as a function of circumferential position away from the boundary, but at r=4.25 Å the displacements are significantly smaller at 90° and larger at about 300°.

(a)

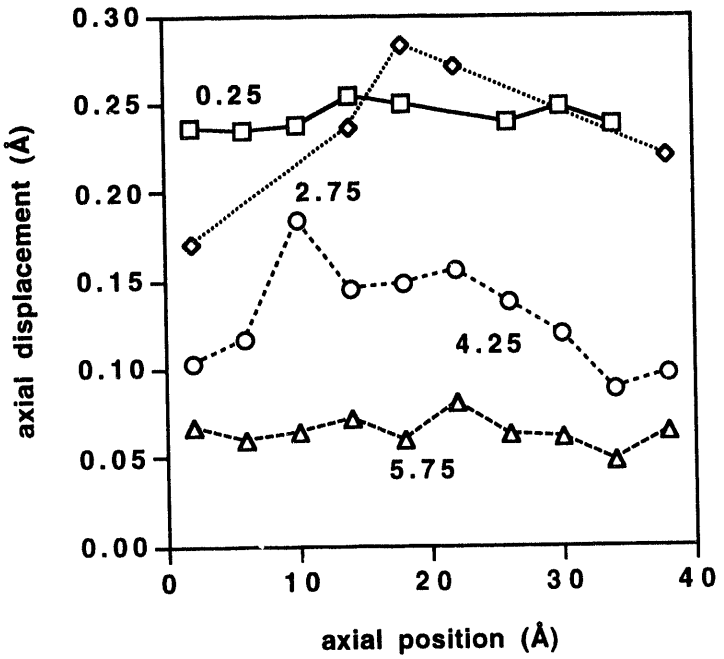

(b)

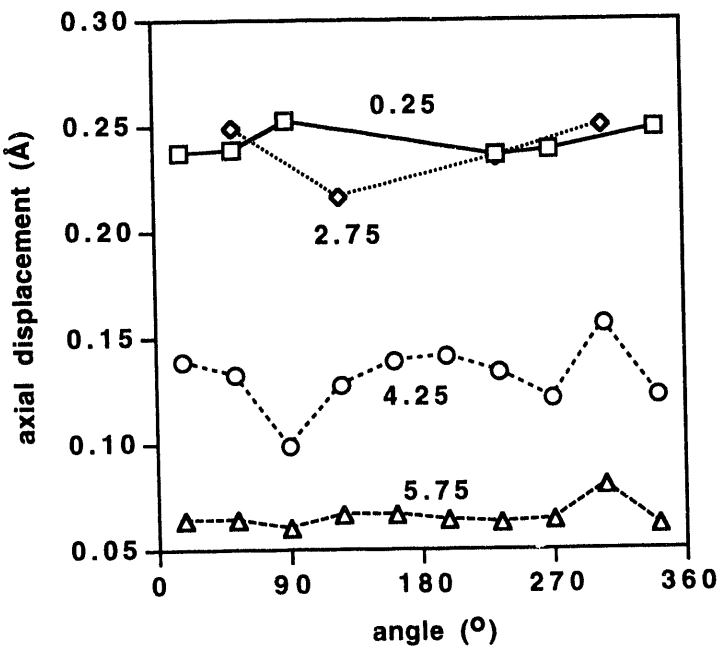

Figure 6 - Axial displacement as a function of (a) axial position and (b) angle for an applied axial force of 0.3 eV/Å/atom. Curves are labeled by radial position (Å). The fiber radius is 5 Å.

SUMMARY

The derivation of the Modified Embedded Atom Method (MEAM) has been presented including a short description of how its parameters are determined. Surface energies and structural energies of a large number of elements are shown to be in good agreement with experiment. Parameters for new MEAM functions for the Si/C system have been determined that fit the properties of Si, C, and SiC quite well. Calculations of a SiC fiber in a diamond matrix show that application of uniform axial forces to the fiber produces non-uniform axial deformation which has been attributed to variation in adhesion at the SiC/C interface.

ACKNOWLEDGMENT

This work was supported by the U. S. Department of Energy under contract No. DE-AC04-94AL85000.

REFERENCES

1. Adams, J. B. and Foiles, S. M., "Development of an Embedded Atom Method Potential for a bcc Metal: Vanadium," *Phys. Rev. B*, Vol. 41, No. 6, 1990, pp. 3316-3328.
2. Baskes, M. I., "Application of the Embedded-Atom Method to Covalent Materials: A Semiempirical Potential for Silicon," *Phys. Rev. Lett.*, Vol. 59, No. 23, 1987, pp. 2666-2669.
3. Baskes, M. I., "Modified Embedded-Atom Potentials for Cubic Materials and Impurities," *Phys. Rev. B*, Vol. 46, No. 5, 1992, pp. 2727-2742.
4. Baskes, M. I., Angelo, J. E., and Bisson, C. L., "Atomistic Calculations of Composite Interfaces," *Modelling Simul. Mater. Sci. Eng.*, Vol. 2, No. 3A, 1994, pp. 505-518.
5. Baskes, M. I., Daw, M. S., and Foiles, S. M., "The Embedded Atom Method: Theory and Application," in *Atomic Scale Calculations in Materials Science*, Tersoff, J., Vanderbilt, D., and Vitek, V. (eds.), MRS, Boston, MA, 1988, pp. 31.
6. Baskes, M. I., Foiles, S. M., and Daw, M. S., "Application of the Embedded Atom Method to the Fracture of Interfaces," *J. de Physique*, Vol. C5, 1988, pp. 483-503.
7. Baskes, M. I. and Johnson, R. A., "Modified Embedded Atom Potentials for hcp Metals," *Modelling Simul. Mater. Sci. Eng.*, Vol. 2, No. 1, 1994, pp. 147-163.
8. Baskes, M. I., Nelson, J. S., and Wright, A. F., "Semiempirical Modified Embedded-Atom Potentials for Silicon and Geranium," *Phys. Rev. B*, Vol. 40, No. 9, 1989, pp. 6085-6100.
9. Bernholc, J., *et al.*, "Mechanism of Self-Diffusion in Diamond," *Phys. Rev. Lett.*, Vol. 61, No. 23, 1988, pp. 2689-2692.
10. Brandes, E. A. (ed.), *Smithells Metals Reference Book*, 6th ed., Butterworths, London, 1983.
11. Car, R., *et al.*, "Microscopic Theory of Atomic Diffusion Mechanism in Silicon," *Phys. Rev. Lett.*, Vol. 52, No. 20, 1984, pp. 1814-1817.
12. Car, R., *et al.*, "Microscopic Theory of Impurity - Defect Reactions and Impurity Diffusion in Silicon," *Phys. Rev. Lett.*, Vol. 54, No. 4, 1985, pp. 360-363.
13. Carlsson, A. E., *Beyond Pair Potentials in Elemental Transition Metals and Semiconductors*, Academic Press, Boston, 1990.
14. Daw, M. S., "Embedded Atom Method: Many-Atom Description of Metallic Cohesion," in *Atomistic Simulation of Materials*, Vitek, V. and Srolovitz, D. (eds.), Plenum Publishing Co., Chicago, 1988, pp. 181.
15. Daw, M. S., "Model of Metallic Cohesion: The Embedded-Atom Method," *Phys. Rev. B*, Vol. 39, No. 11, 1989, pp. 7441-7452.

16. Daw, M. S. and Baskes, M. I., "Semiempirical, Quantum Mechanical Calculation of Hydrogen Embrittlement in Metals," *Phys. Rev. Lett.*, Vol. 50, No. 17, 1983, pp. 1285-1288.
17. Daw, M. S. and Foiles, S. M., "Theory of Hydrogen on Metal Surfaces," in *First International Conference on the Structure of Surfaces*, Van Hove, M. A. and Tong, S. Y. (eds.), Berkeley, CA, 1984, Springer-Verlag, Berlin.
18. Daw, M. S., Foiles, S. M., and Baskes, M. I., "The Embedded Atom Method: A Review of Theory and Applications," *Mater. Sci. Rep.*, Vol. 9, No. 7-8, 1993, pp. 251-310.
19. de Boer, F. R., *et al.*, *Cohesion in Metals Transition Metal Alloys*, North-Holland, Amsterdam, 1988.
20. Finnis, M. W. and Sinclair, J. E., "A Simple Empirical N-Body Potential for Transition Metals," *Phil Mag A*, Vol. 50, No. 1, 1984, pp. 45-55.
21. Foiles, S. M., "Calculation of the Surface Segregation of Alloys Using the Embedded Atom Method," in *Surface Segregation and Related Phenomena*, Dowben, P. A. and Miller, A. (eds.), CRC Press, Boca Rotan, FL, 1990, pp. 79.
22. Foiles, S. M., Baskes, M. I., and Daw, M. S., "Atomistic Studies of Interfacial Structure and Properties," in *Interfacial Structure, Properties and Design*, Yoo, M. H., Clark, W. A. T., and Briant, C. L. (eds.), Materials Research Society, Pittsburgh, PA, 1988, pp. 343-365.
23. Foiles, S. M., Baskes, M. I., and Daw, M. S., "The Calculation of the Equilibrium Interface Structure of Alloys," *Mat. Sci. Forum*, Vol. 37, 1989, pp. 223-234.
24. Foiles, S. M., Baskes, M. I., and Daw, M. S., "Embedded-Atom-Method Functions for the fcc Metals Cu, Ag, Au, Ni, Pd, Pt, and Their Alloys," *Phys. Rev. B*, Vol. 33, No. 12, 1986, pp. 7983-7991.
25. Hirth, J. P. and Lothe, J., *Theory of Dislocations*, McGraw-Hill, New York, 1968.
26. Huang, H., *et al.*, "Molecular Dynamics Determination β-SiC Using Three Representative Empirical Potentials," *in preparation.*
27. Hyland, B., private communication, 1991.
28. Johnson, R. A. and Oh, D. J., "Analytic Embedded Atom Method Model for bcc Metals," *J. Mater. Res.*, Vol. 4, No. 5, 1989, pp. 1195-1201.
29. Korner, A. and Karnthaler, H. P., "Weak-Beam Study of Glide Dislocations in hcp Cobalt," *Phil. Mag. A*, Vol. 48, No. 3, 1983, pp. 469-477.
30. Legrand, P. B., "Relations Entre La Structure Electronique et la Facilite de Glissement Dans Les Metaux Hexagonaux Compacts," *Phil. Mag. B*, Vol. 49, No. 2, 1984, pp. 171-184.
31. Partridge, P. G., "The Crystallography and Deformation Modes of Hexagonal Close-Packed Metals," *Met. Rev.*, Vol. 12, 1967, pp. 169.
32. Rose, J. H., *et al.*, "Universal Features of the Equation of State of Metals," *Phys. Rev. B*, Vol. 29, No. 6, 1984, pp. 2963-2969.
33. Saunders, N., Miodownik, A. P., and Dinsdale, A. T., "Metastable Lattice Stabilities for the Elements," *CALPHAD*, Vol. 12, No. 4, 1988, pp. 351-374.
34. Savino, E. J., Rao, S., and Pasianot, R., "Beyond the Embedded Atom Interatomic Potential," in *Atomic Scale Calculations in Materials Science*, Tersoff, J., Vanderbilt, D., and Vitek, V. (eds.), Materials Research Society, Boston, MA, 1988, pp. 43.
35. Tersoff, J., Vanderbilt, D., and Vitek, V. (ed.), *Atomic Scale Calculations in Materials Science*, 1988, Materials Research Society, Boston, 1988, pp. 471.
36. Tyson, W. R. and Miller, W. A., "Surface Free Energies of Solid Metals: Estimation From Liquid Surface Tension Measurements," *Surf. Sci.*, Vol. 62, 1977, pp. 267-276.
37. Vitek, V. and Srolovitz, D. (ed.), *Atomistic Simulation of Materials*, Plenum Publishing Co., New York, 1989.
38. Wilks, J. and Wilks, E., *Properties and Applications of Diamond*, Butterworth-Heinemann Ltd., Stoneham, MA, 1991.

DATE
FILMED
10/7/94

END